NONLINEAR UNMIXING OF HYPERSPECTRAL IMAGES USING A GENERALIZED BILINEAR MODEL

Abderrahim Halimi, Yoann Altmann, Nicolas Dobigeon and Jean-Yves Tourneret

University of Toulouse, IRIT/INP-ENSEEIHT, 31071 Toulouse cedex 7, France

{abderrahim.halimi,yoann.altmann,nicolas.dobigeon,jean-yves.tourneret}@enseeiht.fr

ABSTRACT

This paper studies a generalized bilinear model and a hierarchical Bayesian algorithm for unmixing hyperspectral images. The proposed model is a generalization of the accepted linear mixing model but also of a bilinear model recently introduced in the literature. Appropriate priors are chosen for its parameters in particular to satisfy the positivity and sum-to-one constraints for the abundances. The joint posterior distribution of the unknown parameter vector is then derived. A Metropolis-within-Gibbs algorithm is proposed which allows samples distributed according to the posterior of interest to be generated and to estimate the unknown model parameters. The performance of the resulting unmixing strategy is evaluated via simulations conducted on synthetic and real data.

Index Terms— Hyperspectral imagery, bilinear model, spectral unmixing, Bayesian algorithm, Gibbs sampler, MCMC methods.

1. INTRODUCTION

Over the last few decades, spectral unmixing has been receiving considerable attention in the signal and image processing literature (see for instance [1] and references therein). The mixture model associated with hyperspectral images can be linear or nonlinear. Linear mixtures known as macrospectral mixtures are interesting when the detected photons interact mainly with a single component on the scene before they reach the sensor. Conversely, nonlinear mixture models result from the interaction of photons with multiple components. Linear mixing models have motivated a lot of research work in the geoscience community. However, nonlinear models constitute a new interesting field of research for hyperspectral imagery. In particular, nonlinear models have shown interesting properties for abundance estimation, e.g., for scenes including mixtures of minerals [2], orchards [3] or vegetation [4].

This paper introduces a generalized bilinear model (GBM) for nonlinear unmixing of hyperspectral images. This model is a generalization of the accepted linear mixing model (LMM) but also of a bilinear model recently introduced by Fan *et al.* in [2]. Estimating the abundances associated to this nonlinear model is a challenging problem. Almost all algorithms dedicated to the unmixing of nonlinear models are based on the least square estimators as in [2]. We propose here a hierarchical Bayesian algorithm to estimate the parameters and hyperparameters associated with the GBM. The major advantage of this algorithm is that it allows one to satisfy the positivity and sum-to-one constraints for the abundances as well as the physical constraint for the nonlinearity coefficients by defining appropriate prior distributions. The joint posterior distribution of these parameters is then derived. However, the minimum mean square error (MMSE) and maximum a posteriori (MAP) estimators associated to this posterior are difficult to derive. We propose to approximate these estimators from samples generated by Markov chain Monte Carlo (MCMC) methods. Note that similar hierarchical Bayesian algorithms have already been applied successfully to linear unmixing of hyperspectral images in [5] and [6].

The paper is structured as follows. Section 2 presents the linear and bilinear models considered in this study. The different components of the Bayesian algorithms associated with these models are studied in Section 3. Section 4 introduces the Metropolis-within-Gibbs sampler which will be used to generate samples according to the joint posterior of the unknown parameters and hyperparameters. Section 5 investigates the behavior of the proposed algorithm when applied to a toy-example, i.e., a single synthetic pixel. Simulation results on real images are presented in Section 6. Conclusions and future works are finally reported in Section 7.

2. SPECTRAL UNMIXING MODELS

According to the LMM, the L-spectrum $\boldsymbol{y} = [y_1, \ldots, y_L]^T$ of a mixed pixel can be expressed as a mixture of R endmembers $\boldsymbol{m}_k$ with additive noise [1]

$$\boldsymbol{y} = \sum_{k=1}^{R} \alpha_k \boldsymbol{m}_k + \boldsymbol{n} = \boldsymbol{M}\boldsymbol{\alpha} + \boldsymbol{n} \tag{1}$$

where $\boldsymbol{M}$ is an $L \times R$ matrix whose columns are the $L \times 1$ endmember spectra $\boldsymbol{m}_k = [m_{1,k}, \ldots, m_{L,k}]^T$ $(k = 1, \ldots, R)$ and $\boldsymbol{\alpha} = [\alpha_1, \ldots, \alpha_R]^T$ is the $R \times 1$ fractional abundance vector. The additive noise $\boldsymbol{n} = [n_1, \ldots, n_L]^T$ is assumed to be an independent and identically distributed (i.i.d) zero-mean Gaussian sequence with variance σ^2.

Nonlinear mixture models account for the presence of multiple photon interactions by introducing additional "interaction" terms in the LMM [3]. The GBM proposed in this paper considers second order interactions between endmember $\#i$ and endmember $\#j$ (for $i, j = 1, \ldots, R$ and $i \neq j$) such that the observed mixed pixel spectrum $\boldsymbol{y}$ can be derived

$$\boldsymbol{y} = \boldsymbol{M}\boldsymbol{\alpha} + \sum_{i=1}^{R-1} \sum_{j=i+1}^{R} \gamma_{i,j} \alpha_i \alpha_j \boldsymbol{m}_i \odot \boldsymbol{m}_j + \boldsymbol{n} \tag{2}$$

where $\odot$ is the Hadamard (term-by-term) product operation, i.e., $\boldsymbol{m}_i \odot \boldsymbol{m}_j = [m_{1,i}m_{1,j}, \ldots, m_{L,i}m_{L,j}]^T$, and with the following constraints for the different parameters

$$\alpha_k \geq 0, \, \forall k \in \{1, \ldots, R\} \quad \text{and} \quad \sum_{k=1}^{R} \alpha_k = 1 \tag{3}$$

$$0 \leq \gamma_{i,j} \leq 1, \, \forall i \in \{1, \ldots, R-1\}, \, \forall j \in \{i+1, \ldots, R\}. \tag{4}$$

Eq. (3) corresponds to the positivity and additivity constraints for the abundances [1]. Eq. (4) provides constraints for the coefficients

$\gamma_{i,j}$ that control the interactions between endmembers $\#i$ and $\#j$ in the pixel. An important property of the GBM is that it reduces to the LMM for $\gamma_{i,j} = 0$ and to the Fan model introduced in [2] for $\gamma_{i,j} = 1$ ($\forall i = 1, \ldots, R-1, j = i+1, \ldots, R$). Moreover, the GBM is particularly well suited to take into account nonlinear effects due to multipaths as explained in [10]. The unknown parameter vector $\boldsymbol{\theta}$ associated with the GBM includes the nonlinearity coefficient vector $\boldsymbol{\gamma} = [\gamma_{1,2}, \ldots, \gamma_{R-1,R}]^T$, the abundance vector $\boldsymbol{\alpha}$ and the noise variance σ^2.

3. HIERARCHICAL BAYESIAN MODEL

This section defines a hierarchical Bayesian model that will be used to estimate the unknown GBM parameter vector $\boldsymbol{\theta} = \left(\boldsymbol{\alpha}^T, \boldsymbol{\gamma}^T, \sigma^2\right)^T$.

3.1. Likelihood

The observation model defined in (2) and the Gaussian properties of the noise sequence $\boldsymbol{n}$ yield

$$f(\boldsymbol{y}|\boldsymbol{\theta}) = \left(\frac{1}{2\pi\sigma^2}\right)^{\frac{L}{2}} \exp\left[-\frac{||\boldsymbol{y} - \boldsymbol{\mu}_{\text{GBM}}||^2}{2\sigma^2}\right] \tag{5}$$

where $\boldsymbol{\mu}_{\text{GBM}} = \boldsymbol{M}\boldsymbol{\alpha} + \sum_{i=1}^{R-1}\sum_{j=i+1}^{R} \gamma_{i,j}\alpha_i\alpha_j \boldsymbol{m}_i \odot \boldsymbol{m}_j$ and $||\cdot||$ is the standard l_2 norm such that $||\boldsymbol{x}||^2 = \boldsymbol{x}^T\boldsymbol{x}$.

3.2. Parameter Prior Distributions

This section details the prior distributions associated with the parameter vector $\boldsymbol{\theta}$. The sum-to-one constraint for the abundances can be encompassed by expressing one abundance α_{k^*} as a function of the others:

$$\alpha_{k^*} = 1 - \sum_{k \neq k^*} \alpha_k. \tag{6}$$

The positivity and sum-to-one constraints (3) are satisfied if $\boldsymbol{\alpha}_{\setminus k^*} = [\alpha_1, \ldots, \alpha_{k^*-1}, \alpha_{k^*+1}, \ldots, \alpha_R]^T$ belongs to the following simplex

$$\mathcal{S}_{\setminus k^*} = \left\{ \boldsymbol{\alpha}_{\setminus k^*} \middle| \alpha_k \geq 0, \forall k \neq k^* \text{ and } \sum_{k \neq k^*} \alpha_k \leq 1 \right\}. \tag{7}$$

The prior for $\boldsymbol{\alpha}_{\setminus k^*}$ is a uniform distribution on the simplex $\mathcal{S}_{\setminus k^*}$ since there is no additional information about this parameter vector.

The parameters $\gamma_{i,j}$ are supposed to be positive as in [3, 4] and less than one reflecting the fact that the interaction abundances are always smaller than the product of the individual abundances. They are also assumed to be *a priori* independent. Assigning a uniform prior on the interval $[0, 1]$ for each coefficient $\gamma_{i,j}$ leads to

$$f(\boldsymbol{\gamma}) = \prod_{i=1}^{R-1}\prod_{j=i+1}^{R} \mathbb{I}_{[0,1]}(\gamma_{i,j}) \tag{8}$$

where $\mathbb{I}_{\mathcal{A}}(.)$ is the indicator function defined on the set $\mathcal{A}$.

It is very common to assign a conjugate inverse gamma prior to the noise variance parameter

$$\sigma^2|\zeta_1, \zeta_2 \sim \mathcal{IG}\left(\frac{\zeta_1}{2}, \frac{\zeta_2}{2}\right) \tag{9}$$

where ζ_1 and ζ_2 are two hyperparameters. For simplicity, we set $\zeta_1 = 2$ and $\zeta_2 = \zeta$ (see [5] for motivations).

3.3. Hyperparameter Prior

A noninformative Jeffreys' prior is finally chosen for ζ, which reflects the absence of knowledge about this hyperparameter [7]

$$f(\zeta) \propto \frac{1}{\zeta}\mathbb{I}_{\mathbb{R}^+}(\zeta). \tag{10}$$

3.4. Posterior distribution of $\boldsymbol{\theta}$

The posterior distribution of the parameter vector $\boldsymbol{\theta}$ can be computed as follows

$$f(\boldsymbol{\theta}|\boldsymbol{y}) \propto \int f(\boldsymbol{y}|\boldsymbol{\theta}) f(\boldsymbol{\theta}|\zeta) f(\zeta) d\zeta \tag{11}$$

where $\propto$ means "proportional to", $f(\boldsymbol{y}|\boldsymbol{\theta})$ is the likelihood function defined in (5) and $f(\boldsymbol{\theta}|\zeta) = f(\boldsymbol{\alpha})f(\boldsymbol{\gamma})f(\sigma^2|\zeta)$ (assuming a priori independence between all the parameters). After substituting the likelihood and the priors in (11) and integrating out with respect to the hyperparameter ζ, the posterior pdf of $\boldsymbol{\theta}|\boldsymbol{y}$ can be written

$$f(\boldsymbol{\theta}|\boldsymbol{y}) \propto \frac{1}{\sigma^{L+2}} \exp\left[-\frac{\|\boldsymbol{y} - \boldsymbol{\mu}_{\text{GBM}}\|^2}{2\sigma^2}\right] f(\boldsymbol{\gamma}) f(\boldsymbol{\alpha}). \tag{12}$$

The MMSE and MAP estimators associated to the posterior pdf (12) are not easy to determine mainly because of the positivity and sum-to-one constraints contained in $f(\boldsymbol{\alpha})$. The next section studies a Metropolis-within-Gibbs algorithm that allows one to generate samples according to the joint distribution $f(\boldsymbol{\theta}|\boldsymbol{y})$ that will be used to estimate the unknown model parameters.

4. METROPOLIS-WITHIN-GIBBS ALGORITHM

This section studies a Metropolis-within-Gibbs sampler which generates samples asymptotically distributed according to the posterior distribution (12). The principle of the Gibbs sampler is to generate samples according to the conditional distributions of the target distribution. When a conditional distribution cannot be sampled directly, it is possible to sample according to a proposal distribution and to accept or reject this sample with an appropriate probability. The resulting algorithm is classically referred to as Metropolis-within-Gibbs algorithm [8] and is detailed below with the following notations: $\boldsymbol{\gamma}_{\setminus(i,j)}^{(t)} = \left\{\gamma_{1,2}^{(t)}, \ldots, \gamma_{i,j-1}^{(t)}, \gamma_{i,j+1}^{(t-1)}, \ldots, \gamma_{R-1,R}^{(t-1)}\right\}$, $\boldsymbol{\alpha}_{i:j}^{(t)} = \left(\alpha_i^{(t)}, \ldots, \alpha_j^{(t)}\right)$ and $\boldsymbol{\alpha}_{\setminus\{k,k^*\}}^{(t)} = \left(\boldsymbol{\alpha}_{1:k-1}^{(t)}, \boldsymbol{\alpha}_{k+1:k^*-1}^{(t-1)}, \boldsymbol{\alpha}_{k^*+1:R}^{(t-1)}\right)$.

4.1. Generating samples according to $f(\sigma^2|\boldsymbol{y}, \boldsymbol{\alpha}, \boldsymbol{\gamma})$

Looking carefully at the joint posterior distribution (12), the conditional distribution of $\sigma^2|\boldsymbol{y}, \boldsymbol{\alpha}, \boldsymbol{\gamma}$ can be determined

$$\sigma^2|\boldsymbol{y}, \boldsymbol{\alpha}, \boldsymbol{\gamma} \sim \mathcal{IG}\left(\frac{L}{2}, \frac{\|\boldsymbol{y} - \boldsymbol{\mu}_{\text{GBM}}\|^2}{2}\right) \tag{13}$$

where $\mathcal{IG}(a, b)$ is the inverse gamma distribution with parameters a and b.

4.2. Generating samples according to $f(\gamma_{i,j}|\boldsymbol{\alpha}, \sigma^2, \boldsymbol{y}, \boldsymbol{\gamma}_{\setminus(i,j)})$

The conditional distribution of $\gamma_{i,j}|\boldsymbol{\alpha}, \sigma^2, \boldsymbol{y}, \boldsymbol{\gamma}_{\setminus(i,j)}$ for $i = 1, \ldots, R-1$ and $j = i+1, \ldots, R$ can be written

$$\gamma_{i,j}|\boldsymbol{\alpha}, \sigma^2, \boldsymbol{y}, \boldsymbol{\gamma}_{\setminus(i,j)} \sim \mathcal{N}_{[0,1]}\left(\frac{\boldsymbol{p}_{i,j}^T\boldsymbol{e}_{i,j}}{\|\boldsymbol{p}_{i,j}\|^2}, \frac{\sigma^2}{\|\boldsymbol{p}_{i,j}\|^2}\right) \tag{14}$$

where

$$\begin{cases} \boldsymbol{p}_{i,j} = \boldsymbol{m}_i \odot \boldsymbol{m}_j \\ \boldsymbol{e}_{i,j} = \boldsymbol{y} - \boldsymbol{M}\boldsymbol{\alpha} - \sum_{l=1,l\neq i}^{R-1} \sum_{p=l+1,p\neq j}^{R} \boldsymbol{\gamma}_{lp}\alpha_l\alpha_p \boldsymbol{m}_l \odot \boldsymbol{m}_p \end{cases}$$

and $\mathcal{N}_{[0,1]}(\cdot,\cdot)$ denotes the Gaussian distribution truncated on the set $[0,1]$. The simulation of samples according to this truncated Gaussian distribution can be performed efficiently by using the method proposed in [9] and detailed in [10].

4.3. Generating samples according to $f(\alpha_k|\boldsymbol{\gamma},\sigma^2,\boldsymbol{y},\boldsymbol{\alpha}_{\setminus\{k,k^*\}})$

The conditional pdf of $\alpha_k|\boldsymbol{\gamma},\sigma^2,\boldsymbol{y},\boldsymbol{\alpha}_{\setminus\{k,k^*\}}$ is given by

$$f(\alpha_k|\boldsymbol{\gamma},\sigma^2,\boldsymbol{y},\boldsymbol{\alpha}_{\setminus\{k,k^*\}}) \propto \exp\left[-\frac{\left\|\boldsymbol{g}_{k,k^*} - \alpha_k\boldsymbol{h}_{k,k^*} + \alpha_k^2\boldsymbol{q}_{k,k^*}\right\|^2}{2\sigma^2}\right]\mathbb{I}_{[0,\alpha_k^+]}(\alpha_k) \quad (15)$$

where α_k^+, $\boldsymbol{g}_{k,k^*}$, $\boldsymbol{h}_{k,k^*}$ and $\boldsymbol{q}_{k,k^*}$ are detailed in [10]. The conditional distribution (15) is not easy to sample. Thus, a Metropolis-Hastings (MH) step is required to generate samples according to the conditional posterior distribution of α_k (see [10] for more details).

5. SIMULATION RESULTS FOR A SYNTHETIC PIXEL

The first experiment considers a synthetic pixel defined as a GBM combination of three pure components (green grass, olive green paint and galvanized steel metal) extracted from the ENVI software library. The abundances have been fixed to $\alpha_1 = 0.3$, $\alpha_2 = 0.6$, $\alpha_3 = 0.1$, and the nonlinearity coefficients to $\gamma_{1,2} = \frac{2}{3}$, $\gamma_{1,3} = \frac{1}{3}$ and $\gamma_{2,3} = \frac{2}{3}$. The observed spectrum has been corrupted by an additive white Gaussian noise with variance $\sigma^2 = 2.8 \times 10^{-3}$ corresponding to a signal-to-noise ratio SNR = 15dB, with $\text{SNR} = L^{-1}\sigma^{-2}\|\boldsymbol{y}-\boldsymbol{n}\|^2$. The unmixing algorithm has been run using $N_{\text{bi}} = 300$ burn-in iterations and $N_r = 700$ iterations to compute the different estimates. The MMSE estimates of the abundances and the corresponding standard deviations are represented as functions of the SNR in Fig. 1. These results have been obtained by averaging the results of 30 Markov chains (for each value of SNR). They are in good agreement with the actual values of abundances (horizontal red lines) especially for high SNRs (note that the actual spectrometers like AVIRIS provide images with SNR levels higher than 20dB when the water absorption bands have been removed). The small deviations between the MMSE estimates and the actual values of the nonlinear abundances $\gamma_{1,2}\alpha_1\alpha_2$, $\gamma_{1,3}\alpha_1\alpha_3$ and $\gamma_{2,3}\alpha_2\alpha_3$ are mainly due to the resemblance between the pure endmembers and some of the "endmember products" $\boldsymbol{m}_i \odot \boldsymbol{m}_j$. However, the effect of these deviations can be neglected because of the small dynamic range of these endmember products, as illustrated by the results reported in Section 6. Note that the convergence issues related to the Metropolis-within-Gibbs sampler have been addressed in [10].

6. SPECTRAL UNMIXING OF AVIRIS IMAGES

This section illustrates the performance of the proposed algorithm when applied to a real hyperspectral dataset. The real image used in this section was acquired over the Cuprite mining site (Nevada,USA) in 1997 by the airborne visible infrared imaging spectrometer (AVIRIS). This area of interest has $L = 189$ spectral bands after removing water absorption bands. It is mainly composed of three $R = 3$ components (muscovite, alunite and cuprite) extracted by the vertex component analysis (VCA) algorithm [11] and depicted in Fig. 2 (top). The abundances of the endmembers have been estimated by running the proposed Bayesian unmixing method on each pixel of the

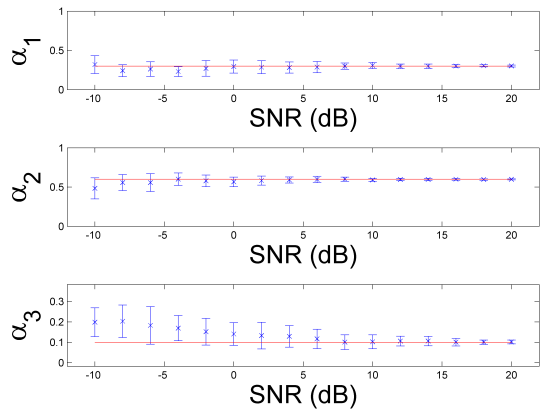

(a) Abundances.

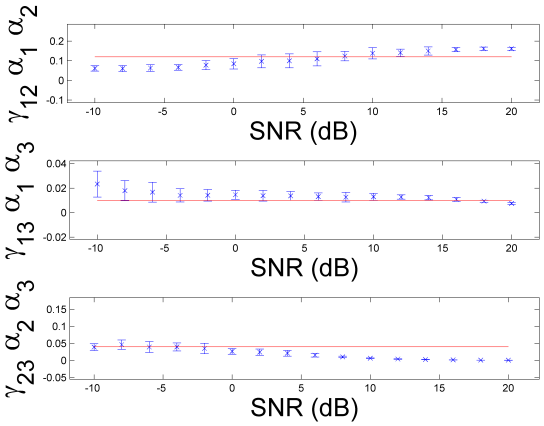

(b) Nonlinearity coefficients.

Fig. 1. MMSE estimates (cross) and standard deviations (vertical bars) of α_1, α_2, α_3 (top), $\gamma_{1,2}\alpha_1\alpha_2$,$\gamma_{1,3}\alpha_1\alpha_3$ and $\gamma_{2,3}\alpha_2\alpha_3$ (bottom) versus SNR.

AVIRIS image. The MMSE estimates of the abundances have been computed by averaging the $N_r = 700$ last generated samples obtained after $N_{\text{bi}} = 300$ burn-in iterations. The image fraction maps, estimated by the proposed method and relative to the linear contribution of the endmembers, are depicted in Fig. 2 (3rd row). Note that a white (resp. black) pixel indicates a large (resp. small) proportion of the corresponding materials. These pictures are visually in good agreement with the abundances obtained when considering a linear model, as illustrated in Fig. 2 (2nd row). However, the proposed algorithm also provides maps for the possible interactions between the materials. These maps are represented in Fig. 2 (4th row). Note that the interaction areas are located in regions where the two components are present as expected.

To compare quantatively our algorithm with other unmixing strategies, we propose two measures of performance. First, the reconstruction error (RE) is used to measure the distance between the measured pixel $\boldsymbol{y}(p)$ and the estimated spectrum $\hat{\boldsymbol{y}}(p)$

$$\text{RE} = \sqrt{\frac{1}{nL}\sum_{p=1}^{n}\|\hat{\boldsymbol{y}}(p) - \boldsymbol{y}(p)\|^2}. \quad (16)$$

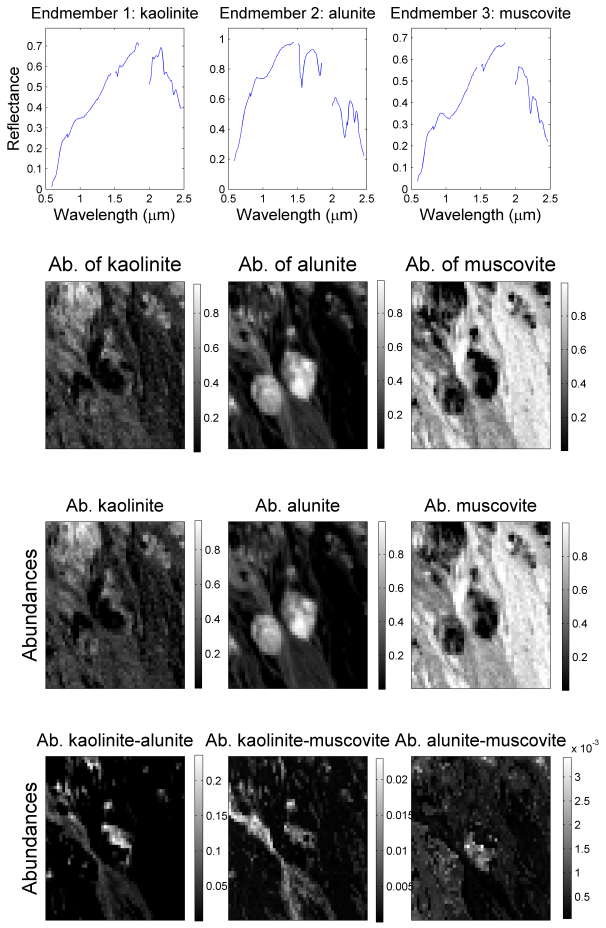

Fig. 2. 1st row: The $R = 3$ endmember spectra obtained by VCA for Cuprite. 2nd row: fraction maps estimated using LMM and a Bayesian algorithm [5]. 3rd and 4th rows: fraction maps estimated according to GBM (linear and nonlinear coefficients).

The spectral angle distance (SAD) defined as

$$\text{SAD} = \frac{1}{n}\sum_{p=1}^{n} \theta\left[\boldsymbol{y}(p), \hat{\boldsymbol{y}}(p)\right] \text{ with } \theta\left[\mathbf{u}, \mathbf{v}\right] = \arccos\left(\frac{\langle \mathbf{u}, \mathbf{v}\rangle}{\|\mathbf{u}\|\,\|\mathbf{v}\|}\right)$$

(where $\arccos(\cdot)$ is the inverse cosine operator) has also been used intensively in the literature. Table 1 shows the unmixing results when the AVIRIS image has been processed using LMM and the Bayesian algorithm [5], LMM and the fully constrained least square (FCLS) algorithm [12], the Fan Model (FM) [2] and the proposed GBM. These results indicate that the GBM yields better performance than the LMM and the FM. Moreover, the GBM provides interaction maps between the endmembers (see Fig. 2, 4th row), contrary to the LMM and FM-based unmixing algorithm. Additional simulations conducted on other hyperspectral dataset are reported in [10]. To summarize, GBM seems to be more flexible than LMM and FM for spectral unmixing (of hyperspectral images) and provides interaction maps between the different spectral components.

Table 1. Comparison of unmixing performance.

	LMM-Bay.	LMM-FCLS	FM	GBM
RE ($\times 10^{-2}$)	2.14	2.11	3.05	1.92
SAD ($\times 10^{-2}$)	3.140	3.130	5.087	2.952

7. CONCLUSION

A new nonlinear model called "generalized bilinear model" was proposed to model the interactions between the macroscopic components of an hyperspectral image. A hierarchical Bayesian algorithm was then proposed to estimate the abundances and nonlinearity coefficients of this nonlinear model. Appropriate priors were chosen to ensure the abundance and nonlinearity coefficients constraints were satisfied. The posterior distribution of the unknown parameter vector was then derived. The corresponding Bayesian estimators were approximated from samples generated using MCMC methods. Results obtained on synthetic and real images illustrated the accuracy of the generalized bilinear model and the performance of the corresponding estimation algorithm. Future investigations include the consideration of spatial correlation between pixels of the hyperspectral image using the proposed generalized bilinear model.

8. REFERENCES

[1] N. Keshava and J. F. Mustard, "Spectral unmixing," *IEEE Signal Processing Magazine*, pp. 44–57, Jan. 2002.

[2] W. Fan, B. Hu, J. Miller, and M. Li, "Comparative study between a new nonlinear model and common linear model for analysing laboratory simulated-forest hyperspectral data," *International Journal of Remote Sensing*, vol. 30, no. 11, pp. 2951–2962, June 2009.

[3] B. Somers, K. Cools, S. Delalieux, J. Stuckens, D. V. der Zande, W. W. Verstraeten, and P. Coppin, "Nonlinear hyperspectral mixture analysis for tree cover estimates in orchards," *Remote Sensing of Environment*, vol. 113, pp. 1183–1193, Feb. 2009.

[4] J. M. Bioucas-Dias and J. M. P. Nascimento, "Nonlinear mixture model for hyperspectral unmixing," in *Proc. SPIE Image and Signal Processing for Remote Sensing XV*, L. Bruzzone, C. Notarnicola, and F. Posa, Eds., vol. 7477, no. 1. SPIE, 2009, p. 74770I.

[5] N. Dobigeon, J.-Y. Tourneret, and C.-I Chang, "Semi-supervised linear spectral unmixing using a hierarchical Bayesian model for hyperspectral imagery," *IEEE Trans. Signal Processing*, vol. 56, no. 7, pp. 2684–2695, July 2008.

[6] O. Eches, N. Dobigeon, and J.-Y. Tourneret, "Estimating the number of endmembers in hyperspectral images using the normal compositional model and a hierarchical Bayesian algorithm," *IEEE J. Sel. Topics Signal Processing*, vol. 4, no. 3, pp. 582–591, June 2010.

[7] H. Jeffreys, "An invariant form for the prior probability in estimation problems," *Proc. of the Royal Society of London. Series A*, vol. 186, no. 1007, pp. 453–461, 1946.

[8] C. P. Robert and G. Casella, *Monte Carlo Statistical Methods*. New York: Springer-Verlag, 1999.

[9] C. P. Robert, "Simulation of truncated normal variables," *Statistics and Computing*, vol. 5, pp. 121–125, 1995.

[10] A. Halimi, Y. Altmann, N. Dobigeon, and J.-Y. Tourneret, "Nonlinear unmixing of hyperspectral images using a generalized bilinear model," *IEEE Trans. Geosci. and Remote Sensing*, 2010, to appear.

[11] J. M. Nascimento and J. M. Bioucas-Dias, "Vertex component analysis: A fast algorithm to unmix hyperspectral data," *IEEE Trans. Geosci. and Remote Sensing*, vol. 43, no. 4, pp. 898–910, April 2005.

[12] D. C. Heinz and C. -I Chang, "Fully constrained least-squares linear spectral mixture analysis method for material quantification in hyperspectral imagery," *IEEE Trans. Geosci. and Remote Sensing*, vol. 29, no. 3, pp. 529–545, March 2001.